Validation of Process Compensated Resonance Testing (PCRT) Sorting Modules Trained with Modeled Data

Julieanne Heffernan[2, b)], Eric Biedermann[2, a)], Alexander Mayes[2, c)], Richard Livings[2, d)], Leanne Jauriqui[2, e)], Siamack Mazdiyasni[1, f)]

[1]*Air Force Research Laboratory (AFRL/RXCA), Wright-Patterson AFB, Ohio*
[2]*Vibrant Corporation, Albuquerque, New Mexico*

[a)] Corresponding author*:* *ebiedermann@vibrantndt.com*
[b)] *jheffernan@vibrantndt.com*
[c)] *amayes@vibrantndt.com*
[d)] *rlivings@vibrantndt.com*
[e)] *ljauriqui@vibrantndt.com*
[f)] *siamack.mazdiyasni@us.af.mil*

Abstract. Process Compensated Resonance Testing (PCRT) combines the collection of broadband resonance data with advanced pattern recognition to produce a fast, accurate, and automated non-destructive inspection for aerospace, automotive, and power generation components. To create a PCRT targeted defect inspection (Sorting Module) the resonance spectra of statistically significant populations of characterized acceptable and unacceptable parts are needed to train PCRT algorithms to recognize the frequency patterns that indicate defects in the midst of normal, acceptable material and geometry variations. In cases where a sufficient number of parts are not available, spectra from physical part populations can be supplemented with 'virtual' spectra generated with PCRT forward models. Previous work investigated the creation of model-trained sorting modules for the detection of creep deformation and crystal orientation for coupon and turbine blade geometries made from single crystal Ni-based superalloy. In this work, model-trained Sorting Modules for crystal orientation and creep deformation were created and then validated with statistically significant populations of physical coupons with and without creep deformation, and with a range of crystal orientations.

INTRODUCTION

Process Compensated Resonance Testing (PCRT) is a non-destructive testing method that utilizes Resonant Ultrasound Spectroscopy (RUS) [1] with advanced pattern recognition algorithms and statistical scoring to perform Pass/Fail nondestructive evaluation (NDE), process monitoring, life monitoring, and material characterization. Resonance inspection is an effective NDE tool because the resonance frequencies of a component relate directly to the component material properties and defect state. In commercial aerospace applications, the use of PCRT defect detection inspections have been shown to have a significant positive impact on field performance [2-4].

Conventional PCRT applications require the collection of statistically significant quantities of measured resonance spectra to establish the resonance frequency effects of normal process variation and train the system to identify diagnostic modes for defect detection. For instance, ASTM Standard Practice E2534-15 [3] describes the configuration and application of PCRT inspections for detection of defects using characterized training sets of components. A broadband resonance spectrum is logged for each component, and the spectrum is designated as 'Good', 'Bad', or 'Unknown' according to the component's classification. Scenarios with limited quantities of training components or incomplete/nonexistent classification can limit the creation of PCRT inspections. However, the modeling tools and techniques developed and demonstrated in this and previous work [6-13] overcome those

limitations by enabling the generation of 'virtual' training sets, with resonance spectra generated by models that predict the effects of material state variation on resonance frequencies.

In previous modeling work [6-13] models of basic and complex geometries were used to create training sets of virtual spectra and configure PCRT targeted defect detection inspections (hence referred to as Sorting Modules). The objective of this study was the validation of model-trained Sorting Modules with a statistically significant population of physical parts. The modeled and physical coupons were made from single-crystal (SX) Mar-M-247, a Ni-base superalloy.

Two Sorting Modules targeting creep deformation and crystal orientation were trained using only virtual spectra, and then validated with the physical coupons. The physical coupons were cast with a wide range of crystal orientations, and creep deformation was produced in a subset of the population with creep testing performed according to ASTM E139. Validation testing comprised a comparison of the frequency change from creep deformation to forward model predictions and inspection of the validation coupons with the model-trained Sorting Modules. The crystal orientation Sorting Module results were compared to Laue X-ray diffraction performed after casting, and the creep Sorting Module results were compared to the deformation recorded during creep testing. Validation with the physical coupons demonstrated that the forward models accurately predicted the resonance frequency effects of crystal orientation variation and creep deformation, and that the Sorting Modules trained with the modeled resonance spectra accurately sorted the physical coupons.

The modeling tools and techniques validated in the work enable the development of PCRT Sorting Modules in the absence of statistically significant and/or fully characterized physical component populations. PCRT Modeling can reduce the time and cost of PCRT Sorting Module deployment and improve Sorting Module accuracy by including more comprehensive populations of acceptable and unacceptable components.

METHODS TO CREATE A PCRT SORTING MODULE

PCRT Sorting Modules are historically trained with a population of physical samples which include examples of acceptable and unacceptable components. Resonance spectra are collected from this training set of components and classified as Good, Bad, or Unknown based on the components' material states. The resonance modes for all parts are aligned into a database and a set of statistical tools are used to configure Sorting Modules. Candidate Sorting Modules are generated and ranked by Vibrational Pattern Recognition (VIPR) algorithms. VIPR first identifies a subset of frequency patterns in the training set that differentiate the acceptable and unacceptable components. The Mahalanobis-Taguchi System (MTS) is used to statistically score the diagnostic frequency resonance peaks for similarity to the acceptable and unacceptable populations and to optimize the number of modes used in the sorting module.

FIGURE 1 shows an example of a VIPR results plot. The MTS limit (x-axis) is the Pass/Fail threshold for similarity to the acceptable (good) training components. The Bias limit (y-axis) is the Pass/Fail threshold for similarity to the unacceptable (bad) training components. Parts that fall within the MTS and Bias limits (lower left quadrant) pass PCRT. Parts that exceed either limit (or both) and fall within any other quadrant, fail PCRT. PCRT Sorting Module inspections typically require between 1-10 seconds per part and return automated Pass/Fail results back to the operator.

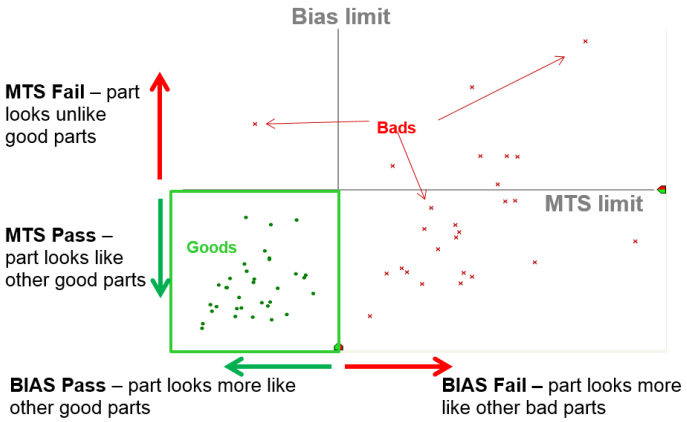

FIGURE 1. Sorting Module Result Plot

The development of PCRT Modeling tools frees Sorting Module generation from its dependence on physical components. Resonance spectra for Sorting Module training can be created via component forward models that predict the effects of material, geometry, and damage variation on component resonance frequencies. The process has been developed over the course of multiple works [6-13] and is summarized in **FIGURE 2.** In step 1, a 3D solid model of the part is created and transferred to a Finite Element (FE) modeling program. In step 2, a series of One-Factor-At-A-Time (OFAT) sensitivity studies are done to quantify the effect of individual geometric, material, or damage parameters and establish distributions of frequency changes for each parameter. In step 3, a series of Monte Carlo (MC) studies use values randomly selected from the OFAT distributions to produce coupled variation in geometric, material, damage, and defect states. The MC studies generate a population of modeled design points with examples of both acceptable and unacceptable parameter values. In step 4, the resonance spectra from the MC studies are imported into standard PCRT software for analysis and Sorting Module generation. The classifications of the spectra are set to 'Good' or 'Bad' based on acceptable or unacceptable parameter variations in the MC design space. In step 5, VIPR algorithms identify frequency patterns in the training set that differentiate the acceptable and unacceptable components. Finally, in step 6, physical parts are tested to validate the model-trained PCRT Sorting Modules. After validation, the Sorting Modules can be used for field testing of physical parts.

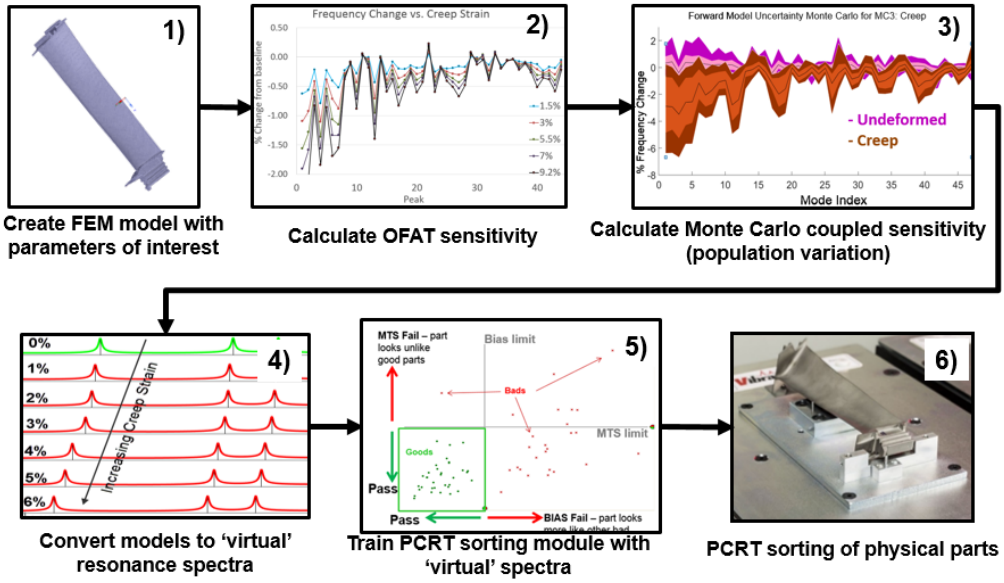

FIGURE 2. PCRT process flow to create Sorting Module from modeled data

MODEL TRAINING SET

A robust training set of resonance spectra will produce a Sorting Module that is not confounded by nominal production variations while maintaining sensitivity to defects of interest. To create a robust training set, a statistically significant number of acceptable and unacceptable parts are needed. The training set must include both the relevant defect characteristics (size, severity, location, etc.) as well as acceptable variations in material and geometry inherent in production.

TABLE 1 summarizes the modeled parameters, parameter ranges, number of design points and classifications used to generate the training sets for each Sorting Module in this study. To create the parts for the modeled training sets, a Monte Carlo (MC) sampling randomly selected combinations of the variables, within the ranges and distributions defined in OFAT studies for each parameter, to generate each design point. Parameter ranges and distributions were determined through a combination of expected machining tolerances, casting variations, and previous modeling and material analysis of SX dogbone populations [13]. Within each range, properties were given normal distributions except for the crystal orientation parameters which were given Weibull distributions based on different levels of casting process control. Hundreds of models were created using the MC method for parameters and classification criteria. The training sets also included modeled "digital twins" of each nominal and crept physical

dogbone by inputting to the model the crystallographic orientation data from Laue measurements, the physical geometric dimensions, and the measured creep strains (if applicable).

TABLE 1. Parameters for model training sets

Sort	Classification	Design Points	Geometric Variation	Material Variation	Crystal Orientation, θ	Creep Strain, %
Crystal Orientation	Acceptable	101	Machining Tolerances + Sample Measurements	E=±1.5% ν=±6.6% A=±4.2% Mass=±0.33% ρ= ±45°	0-10°	0
	Unacceptable	20			10°-20°	0
Creep	Acceptable	198			<10°	0-2
	Unacceptable	82			<10°	2-8

Models were created using the FEM software ANSYS 18.2 (ANSYS, Inc, Cannosburg, PA). A Block Lanczos eigensolver [15] was used to obtain the resonant frequencies for each FE model. First, a dogbone coupon design, **FIGURE 3**, was provided by Metcut Research (Ohio) and the geometry was recreated as a parametrizable CAD geometry. The geometric parameters in this study included the overall length, gauge diameter, and thread lengths. The material was modeled as a nickel-based superalloy (Mar-M-247) in an anisotropic single crystal (SX) state [11]. The material parameters varied in this study included Young's modulus (E), Poisson's ratio (ν), Zener anisotropy ratio (A), and crystal orientation (θ and ρ). Each dogbone had an FE mesh of approximately 246,400 elements and 373,600 nodes.

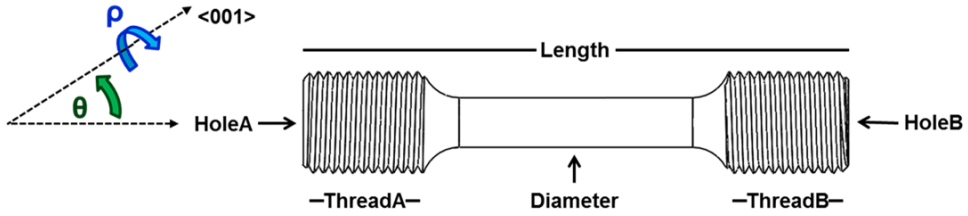

FIGURE 3. ASTM E139-compliant dogbone geometry for validation coupons

Unacceptable modeled parts included simulated creep deformation and/or variation in SX crystal orientation θ. Instead of simulating the complete suite of thermal and mechanical loads that produce creep deformation, a simplified plasticity model was used to produce inelastic deformation. The simplified model produced similar deformations to the more complex model and this approximation also saved considerable computing time. The details of this simplified plasticity model are discussed in prior modeling work [11].

Variation in crystal orientation was modeled by rotating the local element coordinate systems. In the acceptable population, the angle (θ) between the <001> crystallographic axis and the long axis of the dogbone was varied 0-10° using a Weibull distribution representing tight casting control [16,17]. In the bad population, θ varied from 10-20° to simulate out-of-nominal casting defects.

The modeled data was used to create and train two target defect detection Sorting Modules; one for creep detection and one for detection of unacceptable crystal orientation. Because the models were used as virtual training sets, classification criteria were set to distinguish parts with acceptable and unacceptable parameter variation. For instance, literature suggested a tightly controlled SX casting processes would have θ variation less than 10° [14]. Thus, parts modeled with a θ>10° were classified as 'unacceptable' parts. No clear guidelines for acceptable creep threshold values was available, so the acceptability criteria were based on the length tolerance from the dogbone geometric specification. According to Metcut's drawing for the physical samples, the length tolerance for the dogbone geometry was ±1.6%. Vibrant set the threshold for creep damage at 2% strain, meaning that that dogbones with creep strains greater than 2%, would be classified as unacceptable parts.

PHSYICAL VALIDATION SET

The validation set of physical coupons comprised 80 ASTM E139-compliant dogbones described in the previous section. MetCut Research machined the dogbones from 40 cast bars (two dogbones per bar) of SX Mar-M-247. The SX cast bars were purchased from PCC Airfoils, LLC Prototype Foundry. The SX cast bars included a range of crystal orientations (θ, defined in **FIGURE 3**) that were measured using Laue X-ray diffraction at the PCC casting facility. The θ values ranged from 0.4°-37.4°. Approximately half of the samples had θ<10°.

A subset of the original dogbones were sent to Metcut for constant load creep deformation. First an anti-seize compound was added to the threads of the dogbones. Next, the coupons were mounted in a Satec Systems M3 creep load frame, and a three-zone resistance furnace was placed around the coupons. Then the temperature was brought to a constant 950°C. After holding at 950°C for 30 minutes, a uniaxial tensile load of 300MPa was applied on one of the thread sections. The amount of creep deformation was controlled by varying the time spent under the combined thermal and mechanical load. Two extensometers were attached to each end of the dogbone so that during testing, the change in length from the extensometer attachment points was monitored remotely until the desired strain had occurred. Most samples were crept from 0.4-12% strain, as measured along the gauge length. **FIGURE 4** shows an example of the progression of creep strains seen across the dogbones.

FIGURE 4. Progression of creep in physical dogbones

TABLE 2. Physical validation set

Sort	Classification	Part Count	Crystal Orientation*, θ	Creep Strain, %
Crystal Orientation	Acceptable	40	0.4-10°	0
	Unacceptable	40	10-37.4°	0
Creep	Acceptable	15	0.4-10°	0-1
	Unacceptable	17	0.4-10°	2-12
	Borderline	5	0.4-10°	1-2

*As reported by PCC Laue of the cast bars

RESULTS

The first step in the validation of the model trained Sorting Module was the verification of the accuracy of the forward modeling methods for crystal orientation and creep. In a parallel study, a detailed assessment was made between the resonances of each digital twin model to each nominal and crept physical dogbone part [17]. A detailed assessment of the match between modeled and measured resonance spectrum for each dogbone showed the models had excellent match to the physical parts [13]. Also, the accuracy of the creep modeling was verified by comparing the experimentally crept dogbones to their modeled counterparts. For example, **FIGURE 5** compares the change in frequency from the undeformed state to 3% creep strain in dogbone YB2YM-2 and its digital twin. The model (dashed blue line) showed excellent match to the experimental creep strain effects on resonance frequencies (solid orange line) and was considered a good creep model verification.

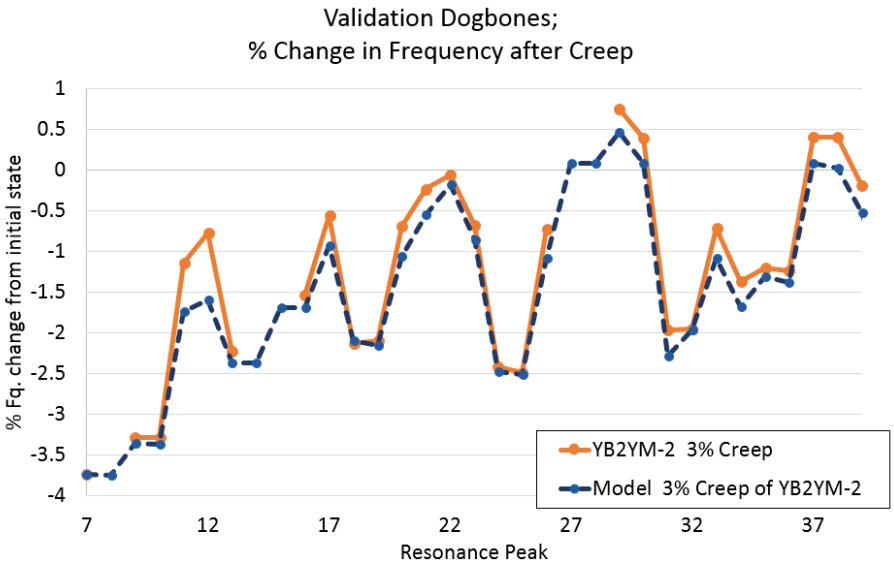

FIGURE 5. % Change in frequency before and after creep; from a physically crept part and its digital twin

Sorting Modules for the detection of crystal orientation misalignment and creep deformation were created using the training sets of resonance spectra from the MC studies as defined in **TABLE 1.** The modeled resonance spectra produced by the MC study were imported into Vibrant's commercial PCRT software. The database enabled a visual comparison of the modeled spectra results and identification of trends. **FIGURE 6** shows an example of five resonance spectra created by the successively modeling of increasing creep strain on a dogbone. As creep strain increased, modes of vibration that were sensitive to creep strain decreased in frequency.

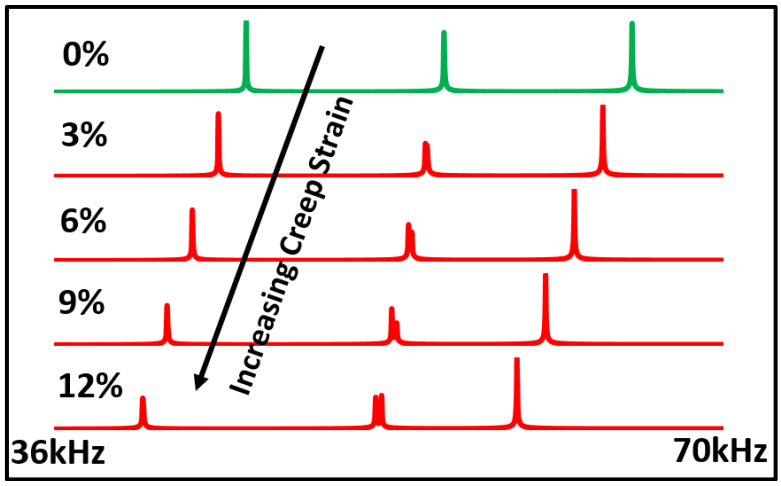

FIGURE 6. Virtual resonance spectra of crept dogbones

PCRT SORTING MODULE FOR DETECTION OF CREEP DEFORMATION

A PCRT Sorting Module was trained to sort dogbones with unacceptable levels of creep from those with acceptable levels of creep. The sort was trained with modeled data (192 samples with acceptable levels of creep, and 82 samples of unacceptable creep). Sample measurements indicated about 1% variation in the length of the gauge section, so samples with <1% creep were included in the 'Good' reference set, and samples with 2% creep or greater were included in the 'Bad' reference set. Samples with creep levels between 1 and 2% were excluded from the algorithm training process.

VIPR identified a Sorting Module that used four diagnostic modes to sort the parts and was chosen for inspection of the validation coupons. The validation coupons that had been creep tested had creep strain values ranging from 0-

12%, described in **TABLE 2**. The VIPR solution plot for the targeted creep detection Sorting Modules is shown in **FIGURE 7** and the results are shown in **TABLE 3**. Each part took approximately 4 seconds to test. The sort successfully rejected 100% of the unacceptable parts (with creep > 2%) and passed all the acceptable parts with creep <1%. It did reject a significant fraction of borderline parts with creep values 1% < creep < 2%. However, this was considered an acceptable result due to the length scale variations of the dogbone populations. According to the drawing specifications for the physical samples, the population of dogbones could have an overall length variation of ±1.6%. As creep is largely a geometric condition, resonance changes due to variation in the length of the dogbone gauge section can be readily confused with elongation due to creep.

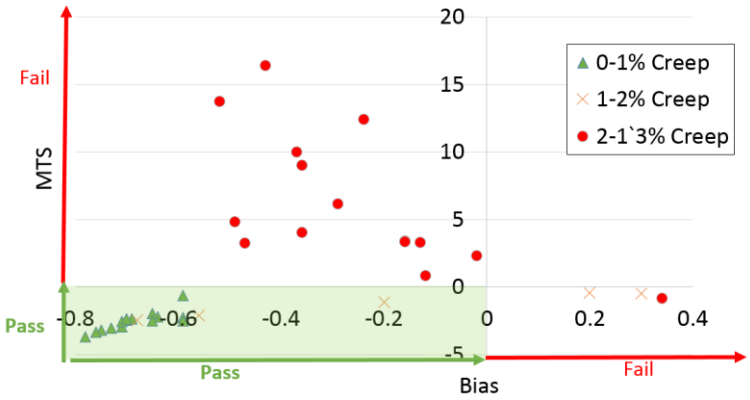

FIGURE 7. Results of creep detection Sorting Module

TABLE 3. VIPR solution results for targeted creep Sorting Module

	Pass PCRT	Fail PCRT
Unacceptable, Creep >2%	0	17
Acceptable, Creep, <1%	15	0
Borderline, Creep 1-2%	3	2

PCRT SORTING MODULE FOR DETECTION OF CRYSTAL ORIENTATION VARIATION

A PCRT Sorting Module was trained to sort dogbones with unacceptable crystal orientation from those with nominal variation. The model training set comprised 101 acceptable samples with crystal orientation θ≤10°, and 20 unacceptable samples with crystal orientation s of θ>10°. The data were then given to the VIPR algorithm to identify which modes best correlated MTS score to θ. VIPR produced several solutions with good correlation that could perfectly segregate the modeled acceptable dogbone from the unacceptable dogbones. The solution with the best correlation used three diagnostic modes to sort the parts and was chosen to inspect the validation coupons.

The VIPR results plot for the targeted crystal orientation Sorting Module is shown in **FIGURE 8**. This VIPR solution took approximately 3 seconds to test each physical part, and every part was tested twice for additional validation. The MTS score (evaluating a part's similarity to the central tendency of the acceptable population) is plotted on the y-axis vs. the θ angle (as-measured on the original cast bars by Laue) on the x-axis. From the physical validation set, there were 40 acceptable parts and 40 unacceptable parts. Testing these parts against the model-trained virtual Sorting Module, **TABLE 4**, correctly sorted all 40 unacceptable parts and 37 of the acceptable parts (three acceptable parts failed the test).

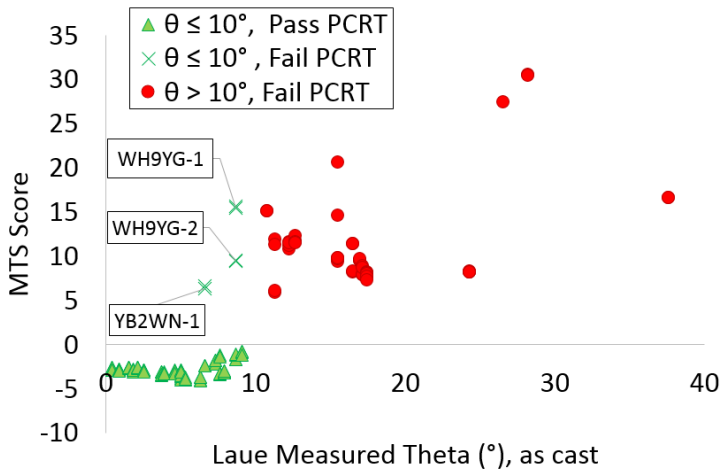

FIGURE 8. VIPR solution for targeted crystal orientation Sorting Module

TABLE 4. VIPR solution results targeted crystal orientation Sorting Module

	Pass PCRT	Fail PCRT
Unacceptable, θ>10°	0	40
Acceptable, θ<10°	37	3

The 37 passing acceptable parts fell below the MTS limit of zero. The three failing acceptable parts, and the 40 failing unacceptable parts fell above MTS = 0. The MTS scores for a large fraction of the unacceptable parts were very high (10+), indicating an extreme effect on the resonance frequencies. There were some signs of a correlation between higher MTS scores and higher θ angles, but this correlation broke down for very high values of θ, and for some dogbones with θ angle between 15° and 20°. These deviations from the general trend were likely due to a combination of effects of θ, Poisson's ratio, anisotropy ratio, and secondary crystal angles like ρ. Part anomalies, like localized secondary grains, could have confounded the Laue measurements, which would also cause deviations from the trend.

Examination of the three misclassified parts showed that their modeled counterparts did not line up well with their measured spectra. Two of them (WH9YG-1 and -2) were a pair from the same bar stock. In a parallel study, resonance inversion of these samples estimated the best fit θ of 13°-14°, quite far from the Laue measurement of the bar at 8.7° [18]. The third misclassified part (YB2WN-1) was notable in that its measured resonance spectrum looked significantly different from that of the other part turned from the same bar (YB2WN-2). Most of the dogbone pairs manufactured from the same bar stock showed a high degree of similarity in their spectra, likely due to having nearly identical crystal orientation. The dissimilarity implied an anomaly within one of the coupons, such as a secondary grain. These results prompted a re-evaluation of the Laue measurements supplied by the casting vendor. Follow-up Laue measurements of the coupons WH9YG-2 and YB2WN-1 found that they did have θ values greater than 10° in at least part of each coupon. WH9YG-1 was not remeasured, but the similarity in spectra and consistency in inversion results between WH9YG-1 and WH9YG-2 imply that -2 also likely had a θ above 10° [17,18].

The corrected VIPR result plot, using the updated Laue measurements, is shown in **FIGURE 9**. When the corrected Laue measurements are used, the Sorting Module shows 100% correct classification (**TABLE TABLE 5**). These results validated the accuracy of the forward models for crystal orientation and the accuracy of the sorting modules trained to detect crystal orientations.

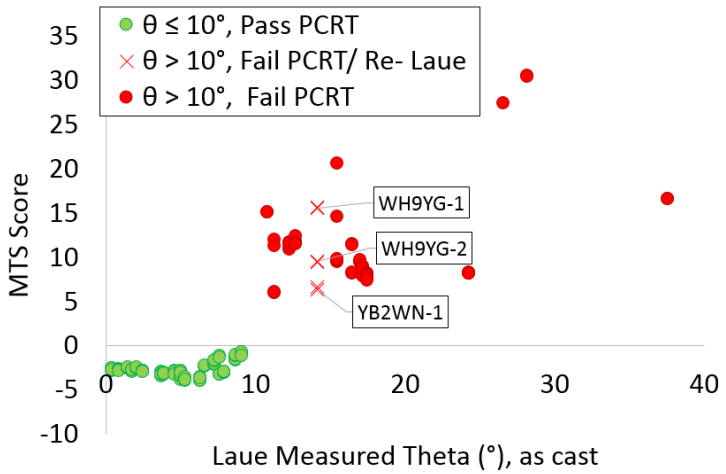

FIGURE 9. Corrected VIPR solution for targeted crystal orientation Sorting Module

TABLE 5. VIPR solution results targeted crystal orientation Sorting Module, after follow-up Laue

	Pass PCRT	Fail PCRT
Unacceptable, θ>10°	0	40
Acceptable, θ<10°	40	0

CONCLUSIONS AND FUTURE WORK

Two model-trained PCRT Sorting Modules, one targeting creep damage and one targeting unacceptable crystallographic orientation, were developed and validated using a statistically significant population of physical parts. The model-based capabilities can significantly reduce PCRT's dependence on data driven training with physical components and can provide more comprehensive material characterization information than ever before. PCRT Modeling tools enable the application of PCRT to components and/or material states that have constraints on the availability of well-characterized, statistically significant training sets of components. The process to produce and validate model based PCRT Sorting Modules has now been defined and demonstrated. Future work includes applying this process to more complex geometries and new material states, and transitioning model-trained Sorting Modules to operational inspections of new and in-service components.

ACKNOWLEDGMENTS

We thank John Aldrin for assistance with modeling methods and inversion techniques. We also thank Brent Goodlet at the University of California Santa Barbra for his help with creep modeling and experimental creep testing. This research was supported by the U.S. Air Force Research Laboratory (AFRL) through a Materials and Manufacturing Director (AFRL/RX) Structural Materials Broad Agency Announcement (BAA) Contract FA8650-15-C-5208 and an AFRL Small Business Innovation Research (SBIR) Phase II Contract, FA8650-15-C-5074. This paper has been cleared for public release by AFRL under case number 88ABW-2018-4923.

REFERENCES

1. Migliori, A., Sarrao, J., Visscher, M. W., Bell, T., Lei, M., Fisk, Z., and Leisure, R., ''Resonant ultrasound spectroscopy techniques for measurement of the elastic moduli of solids,'' *Physica B*, **183**, 1–24 (1993).
2. D. Piotrowski, L. Hunter, and T. Sloan, "Process compensated resonance testing JT8D-219 1st Stage blades," ATA NDT Forum, http://www.vibrantndt.com/wp-content/uploads/75_2008_ATA_NDT_Forum-PCRT_of_JT8D-T1_Blades1.pdf , (2008).

3. D. Piotrowski, G. Weaver, "Enhancing Reliability with Process Compensated Resonance Testing (PCRT) at Delta TechOps" A4A NDT Forum, http://airlines.org/wp-content/uploads/2016/10/9_28_1315.pdf, (2016).
4. D. Craig "NDT Technology Readiness; A P&WC Case Study" A4A NDT Forum, http://airlines.org/wp-content/uploads/2016/11/9_28_1100.pdf, (2016)
5. ASTM Standard E2534-15, "Standard practice for process compensated resonance testing via swept sine input for metallic and non-metallic parts", ASTM International, www.astm.org, (2015).
6. Biedermann, E., Jauriqui, L., Aldrin, J., "Uncertainty Quantification in Modeling and Measuring Components with Resonant Ultrasound Spectroscopy," AFRL-RX-WP-TR-2015-0003 (2015)
7. Biedermann, E., Jauriqui, L., Aldrin, J., C., Goodlet, B., Pollock, T., Torbet, C., Mazdiyasni, S., "Resonance Ultrasound Spectroscopy Forward Modeling and Inverse Characterization of Nickel-based Superalloys," *Review of Progress in QNDE*, Vol. 34, AIP, (2014).
8. E. Biedermann, L. Jauriqui, J. C. Aldrin, B. Goodlet, T. Pollock, C. Torbet, and S. Mazdiyasni, "Resonance ultrasound spectroscopy forward modeling and inverse characterization of nickel-based superalloys," 41st Annual Review of Progress in QNDE, AIP Conf. Proc, 1650, pp. 835-844, (2015).
9. E. Biedermann, J. Heffernan, A. Mayes, R. Livings, L. Jauriqui, J. Aldrin, "Uncertainty Quantification in Modeling and Measuring Components with Resonant Ultrasound Spectroscopy," AFRL-RX-WP-TR-2017-0409 (2017)
10. E. Biedermann, J. Heffernan, A. Mayes, G. Gatewood, L. Jauriqui, G. Goodlet, T. Pollock, C. Torbet, J. Aldrin, S. Mazdiyasni, "Process compensated resonance testing modeling for damage evolution and uncertainty quantification", *43rd Annual Review of Progress in QNDE,* **36**, (2017).
11. J. Heffernan, L. Jauriqui, E. Biedermann, A. Mayes, R. Livings, B. Goodlet, and S. Mazdiyasni, "Process compensated resonance testing models for quantification of creep damage in single crystal nickel-based superalloys," *Materials Evaluation*, 75, n 7, pp. 941-952, (2017).
12. B. Goodlet, C. Torbet, E. Biedermann, L. Jauriqui, J. Aldrin, and T. Pollock, "Forward models for extending the mechanical damage evaluation capability of resonant ultrasound spectroscopy" *Ultrasonics*, **77**, 183-196, (2017).
13. J. Heffernan, E. Biedermann, A. Mayes, R. Livings, L. Jauriqui, B. Goodlet, J.C. Aldrin, S. Mazdiyasni, "Detection and Quantification of Creep Strain Using Process Compensated Resonance Testing (PCRT) Sorting Modules Trained with Modeled Resonance Spectra," 44th Annual Review of Progress in QNDE, AIP Conf. Proc.
14. C-M. Kuo, "Effects of disoriented grains on the elastic constants of directionally solidified superalloys", Materials Science and Engineering, A 494, 1-3-112, (2008).
15. ANSYS Mechanical, Release 18.1.
16. C-M. Kuo "Effects of disoriented grains on the elastic constants of directionally solidified superalloys", *Materials Science and Engineering*, **494**, 1-2, pp. 103-112, (2008).
17. K. Clay, J.D. Jackson, P.N. Quested, and R. Morrell "Improving single-crystal orientation determination for advanced nickel-based alloys", NPL Measurement Good Practice Guide No. 112, National Physical Laboratory, Middlesex, UK, ISSN 1368-6550, (2009).
18. A. Mayes, J. Heffernan, L. Jauriqui, R. Livings, E. Biedermann, J.C. Aldrin, S. Mazdiyasni, "PCRT Inversion for Material Characterization and Digital Twin Calibration," *45th Annual Review of Progress in QNDE*, AIP Conf. Proc., (expected, 2019)